







# Probing bulk electron temperature via x-ray emission in a solid density plasma

K Makur<sup>1</sup>, B Ramakrishna<sup>1,\*</sup> , S Krishnamurthy<sup>1</sup>, K F Kakolee<sup>2</sup> , S Kar<sup>2</sup> ,  
M Cerchez<sup>3</sup> , R Prasad<sup>3</sup>, K Markey<sup>2</sup>, M N Quinn<sup>4</sup>, X H Yuan<sup>5</sup>, J S Green<sup>6</sup>, R H H Scott<sup>6</sup>,  
P McKenna<sup>4</sup> , J Osterholz<sup>3</sup>, O Willi<sup>3</sup>, P A Norreys<sup>7</sup> , M Borghesi<sup>2</sup> and M Zept<sup>8</sup>

<sup>1</sup> Indian Institute of Technology, Hyderabad, Kandi, Sangareddy 502285, India

<sup>2</sup> School of Mathematics and Physics, Queen's University of Belfast, Belfast BT7 1NN, United Kingdom

<sup>3</sup> Institut für Laser-und Plasmaphysik, Heinrich-Heine-Universität, Düsseldorf, Germany

<sup>4</sup> Department of Physics, SUPA, University of Strathclyde, Glasgow, G4 0NG, United Kingdom

<sup>5</sup> School of Physics and Astronomy, Shanghai Jiao Tong University, Shanghai, People's Republic of China

<sup>6</sup> Central Laser Facility, Rutherford Appleton Laboratory, Didcot, Oxfordshire OX11 0QX, United Kingdom

<sup>7</sup> Department of Physics, Atomic and Laser Physics Sub-Department, University of Oxford, Clarendon Laboratory, Oxford OX1 3PU, United Kingdom

<sup>8</sup> Helmholtz Institute Jena, Fröbelstieg 3, 07743 Jena, Germany

E-mail: [bhuvan@phy.iith.ac.in](mailto:bhuvan@phy.iith.ac.in)

Received 12 September 2022, revised 18 January 2023

Accepted for publication 31 January 2023

Published 22 February 2023



CrossMark

## Abstract

Bulk electron temperatures are calculated for thin Cu targets irradiated by the petawatt class Vulcan laser, from the  $K\alpha$  yield obtained using highly oriented pyrolytic graphite crystals. Cu- $K\alpha$  emission studies have been used to probe the bulk electron temperature. A 30–80 eV core temperature extends homogeneously over distances up to ten times the laser focal spot size. Energy shifting has been observed due to different ionization states produced for different temperatures in the plasma. Polarization dependencies of plasma temperature are observed through the production of x-rays in different targets. 2D PIC simulations were performed to measure the polarization dependency of bulk electron temperature, which supports our experimental results. This paper could be of importance in understanding the different behavior of laser coupling at different polarizations and their role in x-ray production.

Keywords: laser plasma, bulk electron temperature, K alpha, polarization

(Some figures may appear in colour only in the online journal)

## 1. Introduction

With the advent of the chirped pulse amplification technique [1], high-intensity lasers are easily accessible. Various phenomena, such as table-top ion acceleration [2], and high energetic ultra-short photon beam generation [3] have been observed through relativistic plasma production at high temperatures. The laser gets absorbed through different processes such as resonance absorption [4], vacuum heating [5], hole boring [6], and  $J \times B$  heating [7], depending on the

incident laser intensity. However, there could be multiple absorption mechanisms applicable, at relativistic intensities ( $I > 10^{18} \text{ Wcm}^{-2}$ ), the most dominant mechanism is the  $J \times B$  heating, where the fast electrons are generated along the laser propagation direction. The interaction of intense, ultra-short laser pulses with matter allows the generation of plasmas at a solid density at high temperatures. Under these conditions, the ion coupling parameter  $\Gamma$  [8] exceeds one, and the plasma is thus in a strongly coupled state [9]. Such warm dense plasmas are particularly of interest in inertial confinement fusion (ICF) and astrophysics [10]. For example, it is possible to study the x-ray opacity of matter under conditions found in stellar interiors [11]. High energy-density laser-produced

\* Author to whom any correspondence should be addressed.

plasmas offer a unique window for investigating thermal equilibration between electrons and ions in strongly coupled plasma.

The laser transfers most of the energy at the critical density surface where the hot electrons are produced and accelerated through the ponderomotive force. Hot electrons gain energy up to a few MeV leading to a range larger than the target thickness. While traveling through a cold target, these hot electrons knock electrons out of the inner shell of the target atoms. Subsequently, electrons from the higher energy shell jump to the lower energy shell to fill the vacancy resulting in characteristic x-ray emission. X-ray probing of dense plasma is frequently employed in high-energy-density experiments [12, 13]. The study of  $K\alpha$  emission from dense plasma can give insight into the propagation dynamics of electrons in metallic targets, which is essential for the development of schemes, such as fast ignitor fusion [14] as well as for ultrashort x-ray sources. The scientific community is interested in the production of such short-pulse x-ray beams, as they can be used in a variety of experimental techniques, such as ultra-fast diffraction [15] study from dynamically compressed solids, or x-ray scattering [16] from non-equilibrium dense plasmas. Furthermore, the analysis of the  $K\alpha$  x-ray emission can yield valuable information about the conditions within the target interior during and immediately after the interaction, since the lifetime of the emission is within a few picoseconds, well below the typical hydrodynamic expansion time, and suffers insignificant attenuation in the solid density plasma [17, 18]. In particular, analysis of the emitted x-rays can provide information on the bulk electron temperature, providing crucial information on the plasma conditions. The influence of warm and dense plasmas on the emitter plays an important role in line emission transition, with the transition depending on the bulk electron temperature and electron density. At higher temperatures, some of the electrons from the L and M shells could be depleted, which gives the shifting of the spectral lines due to higher ionization states. In the work of Gregori *et al*, it is shown how the temperature and ionization state of the bulk target gives rise to spectral shifting [19]. In the same note, P Neumayer reported the blue shifting of the x-ray lines from the mass limited Chlorinated plastic target due to the isochoric heating of the order of 18 eV [20]. In both of the experiments mentioned above the laser energy increased to change the temperature of the target and corresponding spectral shift was observed for various laser energies.

Polarization effects on the ion acceleration are already observed, where the ion phase space is orderly and stable for the case of circularly polarized (CP) laser light due to the lack of heating via  $J \times B$  heating [21–24] mechanism. There is a strong correlation between plasma electron heating and the polarization of the incident light. At intensities above relativistic intensities,  $v \times B$  force has the same order as the force governed by the laser electric field, which should be taken into consideration. With this additional term, the ponderomotive force can be written as [25–27],

$$\vec{F}(r) = -\frac{e^2}{4m_e\omega^2} \nabla \langle E^2 \rangle \left( 1 + \frac{1-\epsilon^2}{1+\epsilon^2} \cos(2\omega t) \right) r\hat{r} \quad (1)$$

where,  $e$ ,  $m_e$  are the charge and rest mass of the electron respectively,  $\omega$  is the angular frequency of the laser beam and  $\epsilon$  stands for the polarization ellipticity value that varies from 0 to 1 depending on the degree of polarization. The first term of the above equation represents the component of the force that pushes the electrons from regions of higher electric field to lower electric fields. The second term is called the  $J \times B$  heating [25] effect, which stimulates electron oscillation with a frequency twice the laser frequency. For linearly polarized (LP) light the value of the ellipticity ( $\epsilon$ ) is 0, which makes the second term in the equation significant. Whereas, for CP, the value of  $\epsilon$  is 1, which makes the second term zero. This extra heating in LP pulses leads to electrons flying away quickly from the interaction region. In contrast to LP pulses, for CP pulse electron heating in the plasma is strongly suppressed owing to the absence of the oscillating component in the  $\sim v \times B$  force. Instead, electrons are compressed to a highly dense layer piling up in front of the laser pulse. By choosing the laser intensity, target thickness, and density such that the light pressure equals the restoring force given by the charge separation field, the whole focal volume eventually propagates ballistically as a quasi-neutral plasma bunch, continuously gaining energy from the laser field. In this scenario, all particle species are accelerated to the same velocity, which intrinsically results in a monochromatic ion spectrum. As long as the electron temperature is kept low, a phase-stable acceleration can be maintained, and the process is expected to lead to very high conversion efficiencies and ion maximum energies scaling linearly with laser intensity under optimum conditions. The detailed analysis and simulation results are shown in the previous studies [21, 23, 28].

When the laser interacts with any target, it is the ponderomotive force which accelerates the electrons within the target, and these electrons which gain high kinetic energy are termed as hot electrons. From equation (1), it is clear that the CP laser will have a reduced ponderomotive force compared to that for the LP laser, mainly due to the suppression of  $J \times B$  heating mechanism for the CP laser. Consequentially, the LP laser gives rise to a higher temperature in the hot electrons compared to the CP laser. Eventually, these hot electrons transfer the energy to the bulk target through the collisional energy transfer, therefore different laser polarization will lead to a different bulk target conditions. The x-rays generated from this bulk target are used as a tool to infer about the temperature of the bulk target. The x-ray emission from highly charged plasma has proven to be a reliable diagnostic for plasma parameters, such as temperature and electron density distribution. In our work, Cu- $K\alpha$  from ionized Cu plasma is used to measure the plasma temperature and ionization of the plasma state. The change in the ionic potential due to the different charge distributions in the K shell and M shell results in the shifting and broadening of the spectral lines.

## 2. Experimental details

The experimental investigation of the measurement of electron temperature in the bulk plasma as a function of laser

polarization inferred from the shifting of characteristic transition lines was achieved by employing one-dimensional imaged spectroscopy of Cu-K $\alpha$  doublet via highly oriented pyrolytic graphite (HOPG) crystal spectrometer [29–31]. HOPG crystals consist of many small, perfectly aligned crystallites, making them highly efficient for x-ray diffraction over several keV ranges. The mosaic spread of the crystal increases the reflectivity of the incident beam. Spectrometer works on the principle of Bragg's law, where different energetic photons get diffracted from the crystal at different positions on the image planes.

The experiment was performed at Rutherford Appleton Laboratory employing the VULCAN petawatt laser system. The laser delivered  $\sim 150$  J energy on target in pulses of 700 fs–900 fs FWHM duration after being reflected off a plasma mirror (PM), resulting in an intensity contrast ratio of  $10^9$  between the main pulse and the ns long amplified spontaneous emission (ASE). The laser was focused to around  $5 \mu\text{m}$  on Cu targets of varying thicknesses at normal incidence by an  $f/3$  off-axis parabolic mirror with an intensity  $\sim 5 \times 10^{19} \text{ W cm}^{-2}$ . The polarization of the laser on the target varied from linear (LP) ( $\varepsilon = 0$ ) to nearly circular (CP) ( $\varepsilon \sim 1.14 \pm 0.04$ ) by employing a zero-order quarter-wave plate placed between the focusing optics and the PM. Here,  $\varepsilon$  is the ratio between the laser electric field amplitudes along the vertical and horizontal axes, as determined by the combined effect of the wave plate and of reflection from the PM.

The primary diagnostic to measure the electron temperature is Cu-K $\alpha$  radiation emitted at the rear side of the target. The changes introduced in the spectral shape infer the plasma parameters, such as temperature and electron density distribution. The source size of the emitting region is diagnosed using an x-ray pinhole camera (with resolution set by  $25 \mu\text{m}$  pinhole diameter), and via source broadening using a HOPG spectrometer ( $\sim 30 \mu\text{m}$  resolution). The pinhole camera had  $25 \mu\text{m}$  pinholes, filtered to select different spectral ranges in the range of 1.7–10 KeV and an image plate as a detector. We need to address these questions very well.

The HOPG crystal provided data on the relative K $\alpha$  yield of the targets as well as an independent measure of radial source size due to a spectral linewidth dominated by source broadening. HOPG is particularly suited for this experiment because its unique crystal plane structure combines highly efficient x-ray diffraction and mosaic para focusing [32]. The spectrometer design employs a ZYA type flat HOPG crystal, with mosaic spread  $\gamma = 0.40$ , 25 mm wide in the sagittal (non-dispersion) direction and 50 mm long in the meridian (dispersion) direction. The thickness of the crystal is 2 mm. For para focusing to happen, both the source of crystal and crystal to image plate maintained the same distance of 250 mm. The spectrometer dispersed the incoming x-rays onto image plates (Fuji film Bas TR) filtered with  $25 \mu\text{m}$  of Al. For the thicker crystal, due to the deep penetration within the bulk crystal, the beam becomes more wider after the reflection. Taking a thinner HOPG crystal is always a good idea to increase the resolution of the spectrometer. The thinner target and longer source-to-crystal distances increase the resolution of the spectrometer.

The spectrometer is fully shielded with lead to prevent a direct line of sight between the plasma source and the detector. There is an excellent agreement between the source sizes inferred from HOPG and the pinhole imaging.

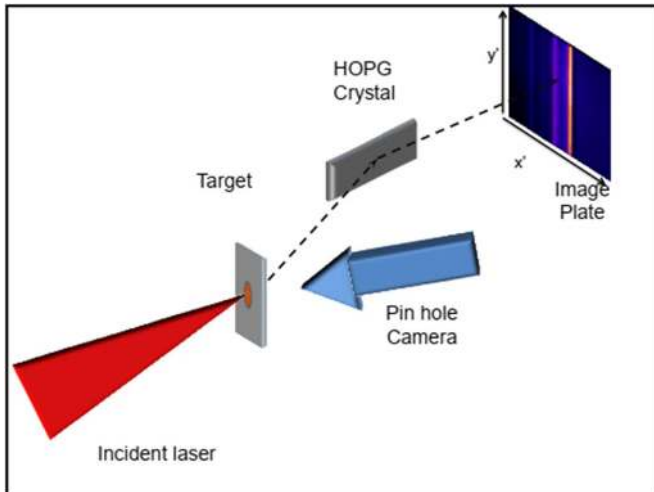
### 3. Results and discussions

The HOPG crystal spectrometer yields 1D resolved spectra of the circular plasma emission source, as shown in figure 1. Figure 2 shows the x-ray spectra for the Cu 500 nm target corresponding to the CP and LP laser pulses. The observed K $\alpha_1$  and K $\alpha_2$  from 500 nm Cu targets are  $8052.3 \pm 1.6$  eV and  $8034.3 \pm 1.6$  eV for CP pulses and  $8071.3 \pm 1.6$  eV and  $8052.3 \pm 1.6$  eV for LP pulses respectively. The shifting of the energy for both the polarizations is shown with reference to cold Cu lines (K $\alpha_1$ —8047.8 eV and K $\alpha_2$ —8027.8 eV). Along with the shifting of K $\alpha$  lines, the x-ray flux is also observed to be different for different polarizations.

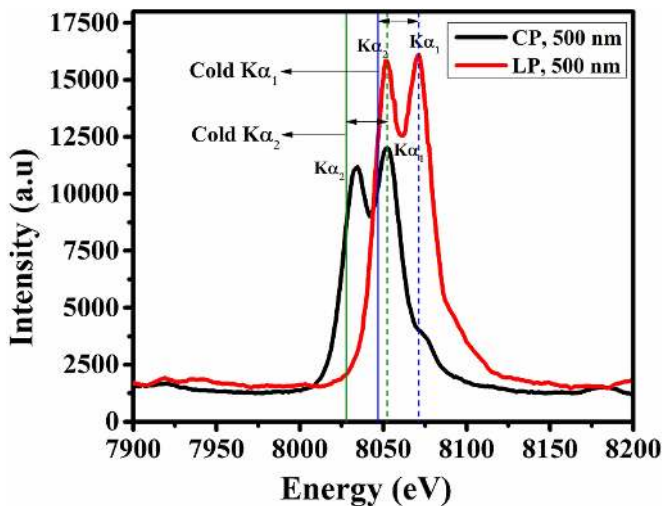
The measured Cu-K $\alpha$  peaks obtained for CP and LP pulses are fitted using the radiation code FLYCHK [33] to obtain the bulk electron temperatures and ionization states. The fitting was achieved by varying the bulk electron temperature (5 eV to 100 eV) and the total electron density ( $10^{21}$ – $10^{22}$ ). Before the main pulse, the pre-pulse interacts with the flat cold target, and a steep density plasma is produced within the target. The temperature distribution of electrons is spatially varying within the plasma due to the dependence of the absorption of laser energy within a steep density gradient plasma produced by the pre-pulse. The laser starts to penetrate at the critical density surfaces, and the hot electrons produced at the critical density travel through the rear side of the target. With this consideration, in our Flychk simulation, the density of the electrons were taken to be  $\sim 10^{21} \text{ cm}^{-3}$  which is the critical density corresponding to the laser wavelength. The hot electron temperature is kept constant at 820 KeV, which is the obtained hot electron temperature from the scaling law [34] corresponding to our laser parameters. A hot electron fraction in the entire plasma was considered to be 0.005% of a total population of electrons at the MeV range is consistent with the relative volumes of the, directly and indirectly, heated plasmas [35]

Figure 3 gives the best FLYCHK fitting for the experimentally obtained Cu-K $\alpha$  spectrum from the 500 nm Cu target for both the polarization of the laser. Using FLYCHK, the spectrum was fitted to extract the temperatures of the bulk electrons and the ionization population within the plasma.

We can see from the figures that both the experimentally obtained spectrum (K $\alpha_1$  and K $\alpha_2$ ) are well-matched with the spectrum obtained from simulations. From figure 3, it is clear that the energies are blue-shifted for LP compared to CP for the same target and laser conditions. Further, the FLYCHK model fitted to the experimental data confirms a reduction in bulk electron temperature from 75 eV (LP) to 32 eV (CP). Though the energy lines are well matched, there is a little discrepancy in the matching of the intensity peaks of the K $\alpha_2$  line. A possible reason for not exactly fitting the K $\alpha_2$  peak is the exclusion of the effect of the Stark effect and Doppler broadening



**Figure 1.** Schematics of the experimental layout for the Cu- $K\alpha$  x-ray diagnosis using a HOPG spectrometer.



**Figure 2.** Comparison of experimentally observed spectrum for linear and circularly polarized pulses on a 500 nm Cu target. Blue and green solid lines represent the cold  $K\alpha_1$  and  $K\alpha_2$  lines respectively. The blue shifting of energy is observed for both LP and CP cases with respect to the cold  $K\alpha$  lines.

in the Flychk code for the Cu ( $Z = 29$ ) target. The line shape and line intensity are dependent on the Stark effect and Doppler effect. Flychk includes the Stark broadening and Doppler broadening effects till the atomic number  $Z = 26$ . Therefore, in our case ( $Z = 29$ ), the Flychk model gives rise to the observed difference in the line shape. Another possible reason for this mismatch of the  $K\alpha_2$  intensity is the depletion of the energy levels due to the temperature.  $K\alpha_1$  is emitted when an electron jumps from the  $2P_{3/2}$  to  $1s$  state, while the transition of electrons from  $2P_{1/2}$  to  $1s$  gives rise to  $K\alpha_2$ . For pure cold targets, it is always expected that  $K\alpha_1$  intensity to be more intense than that of  $K\alpha_2$ . Theoretically, the intensity ratio should be 2:1 due to the higher multiplicity of the  $2P_{3/2}$  state. In our observation, the x-ray is not emitted from a pure cold target, but from an ionized warm dense plasma. Due to this ionization, some of

the energy levels become depleted. Considering this depletion, the  $2P_{3/2}$  energy level will be more depleted of electrons compared to  $2P_{1/2}$ . This depletion of electrons could be one of the reasons for not matching the experimentally obtained value of intensity to the theoretical value. Although this explanation is reasonable, it requires the ionization state to reach  $19+$  which is slightly above the obtained charge state from Flychk. This feature needs to be addressed with a greater detail to arrive at a conclusion. Nevertheless, the changes in the intensity of  $K\alpha_1$  and  $K\alpha_2$  lines are solely dependent on the electron population. Though the intensity of the two lines is not completely reproduced from the simulations, it does not affect the obtained physical parameters because only energy shifting is considered as the reference and the energy is exactly matched.

Using Flychk, the fitting was done by varying the bulk electron temperatures for a given density. The extracted temperature is sensitive to density. The density of the rear side of the target will be in the range of critical density ( $n_c$ ) to the solid density target. Here, the critical density ( $\sim 10^{21}$ ) is considered for extracting the temperature and mean ion population. However, if the target is considered as a nearly solid density target, the fitted temperature for the LP target turned out to be 91 eV and for the CP target, it changed to 42 eV. As expected, for a solid density target, the required temperature would be higher to reach the same ionization state. It is not feasible to determine the exact density, which corresponds to the emitted x-ray, but it is always expected to be in the range of near critical density to solid density. Although there is some fitting uncertainty, our obtained results do not vary widely with change in density.

Figure 4 represents the ion population distribution corresponding to the fitted energy obtained from FLYCHK simulations for both the polarization states for the same laser and target parameters. In this case, we observe different ionizations in the cold target for different polarization states of the laser pulse. These different ionization states of the bulk target at two different polarizations lead to the shifting in the Cu- $K\alpha$  spectrum (shown in figure 2).

The difference in temperature between LP (75 eV) and CP (32 eV) gives rise to a corresponding shift in the energy of 19 eV and 18 eV for Cu- $K\alpha_1$  and Cu- $K\alpha_2$  respectively for LP compared to CP. The shifting of the  $K\alpha$  spectrum is attributed to the heating of cold electrons, which results in further ionization of the plasma resulting in the screening effect. The main reason for the shifting of spectral lines is associated with the laser polarization. As the bulk electrons gain energy from the hot electrons via collisions, the increase in hot electron temperature would cause an increase in the bulk electron temperature as well. The LP laser transfers relatively higher energy to the hot electrons, the hot electrons would have a range greater than the typical target thickness and the refluxing due to the self-generated electric field confines the electrons within the target. As a result, the bulk target gets heated more in the case of LP compared to the CP case.

As the temperature of the bulk target increases, ionization within the bulk target also increases. This ionization of electrons from the outer shells reduces the screening of the inner shell electrons from the outermost electrons. The reduced repulsive force between the outermost electrons for the higher

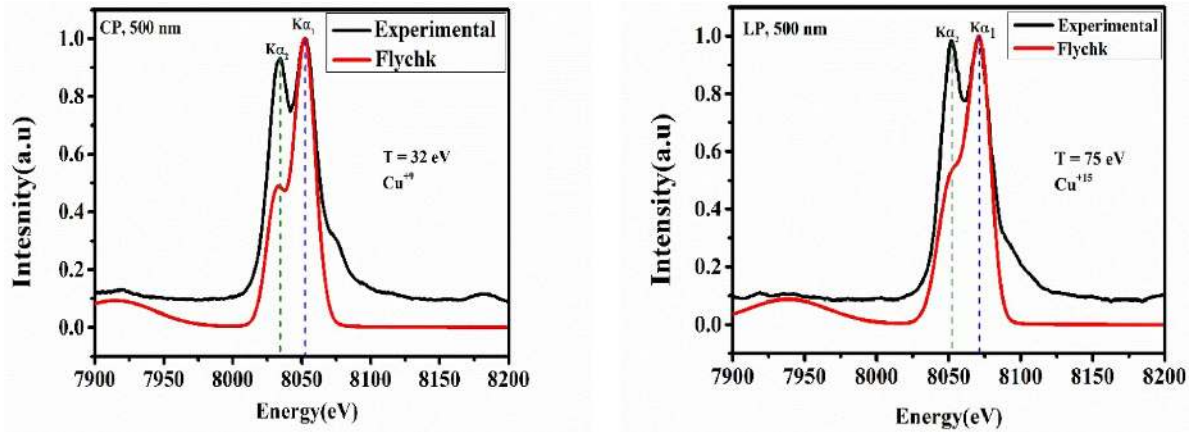


**Figure 3.** FLYCHK fitting of the experimentally obtained spectra. The temperature extracted from FLYCHK for the case of circular polarization (left) and linear polarization (right) is about 32 eV and 75 eV respectively.

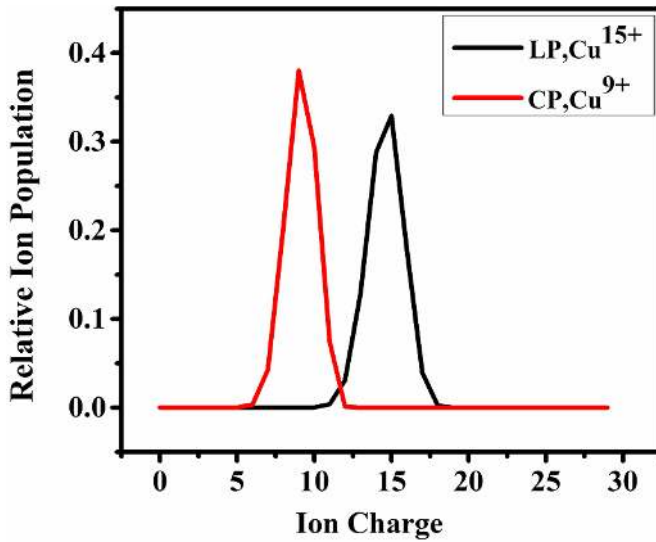


**Figure 4.** Comparison of ion charge distributions obtained from FLYCHK fitting, corresponding to different polarization states of the laser for a 500 nm Cu target.

ionization states increases the attractive potential of the inner electrons and makes the inner electrons more tightly bound to the nucleus. If an electron jumps from  $n_2$  to  $n_1$  and the energy of the photon will be in accordance with the Bohr formula given below,

$$E = h\nu = -13.6 Z^2 \left( \frac{1}{n_1^2} - \frac{1}{n_2^2} \right) \quad (2)$$

where  $Z$  is the effective nucleon number and  $(n_1, n_2)$  are the principal quantum numbers to represent the initial and final states of the electron respectively. From the above equation, it is seen that the energy of the photon depends on the quantum states and the  $Z$  values. The value of  $Z$  is constant only for pure cold atoms, this value changes with the ionization of the atoms. The value of  $Z$  determines how the outermost electrons affect the nuclear potential. With the inclusion of the screening

effect,  $Z$  is replaced by  $Z_{\text{eff}} = Z - \sigma$ , where  $\sigma$  is the screening factor, which determines the energy of the transitions and is different for different ionization states for a single atom. The shifting of the energy is larger for higher charged states. As a result, the photon emission energy for the transition of  $2P$  to  $1S$  increases.

Up to now, we have observed the shifting of the energy lines due to different ionization states of the bulk target. It is observed from figure 2 that, there is a difference in the  $K\alpha$  x-ray intensity for two different polarizations. The x-ray intensity is higher for the LP case compared to the CP case. The additional heating in the case of LP produces a larger number of hot electrons, further leading to an increase in the interaction with the bulk target, resulting in higher x-ray production.

In summary, different ionization states have been observed due to different temperatures generated for different polarization states of the laser. The primary reason for the different temperatures for different polarization states is due to the reduction of  $J \times B$  heating in the case of CP light. From equation (1), it is clear that the second term remains finite for LP lasers giving rise to additional heating contributing to higher ionization states of the target. The smoothening of the entire line shape is mainly observed due to the contribution of Stark broadening. It is shown that the range of hot electrons is substantially reduced compared to the single-particle range [36] by the electrostatic field required to drive the return current and that the observed range depends on an electron distribution function and absorption fraction, making precise estimates of the bulk electron temperature difficult. This is consistent with recent studies suggesting reduced bulk electron temperature interactions with a steep density gradient [37] which are expected for our experimental parameters due to the use of a PM combined with ponderomotive steepening [38, 39]. A direct comparison of the  $K\alpha$  yield obtained for 500 nm Cu targets show that within the shot-to-shot fluctuations the maximum temperature varies between 30 and 80 eV for circular and linear polarization, respectively.

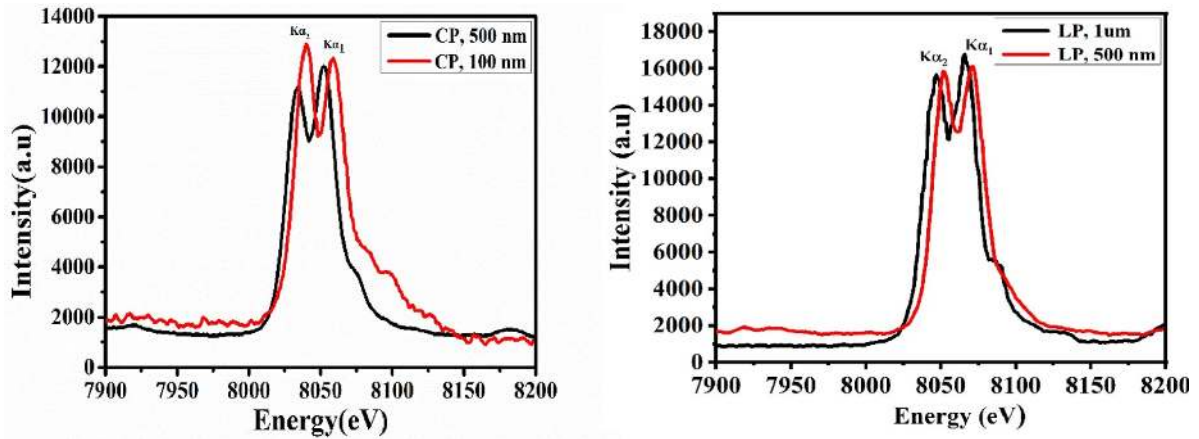


**Figure 5.** Experimental observation of variation of x-ray emission from targets of different thicknesses interacting with a laser pulse with circular polarization (left) and linear polarization (right).

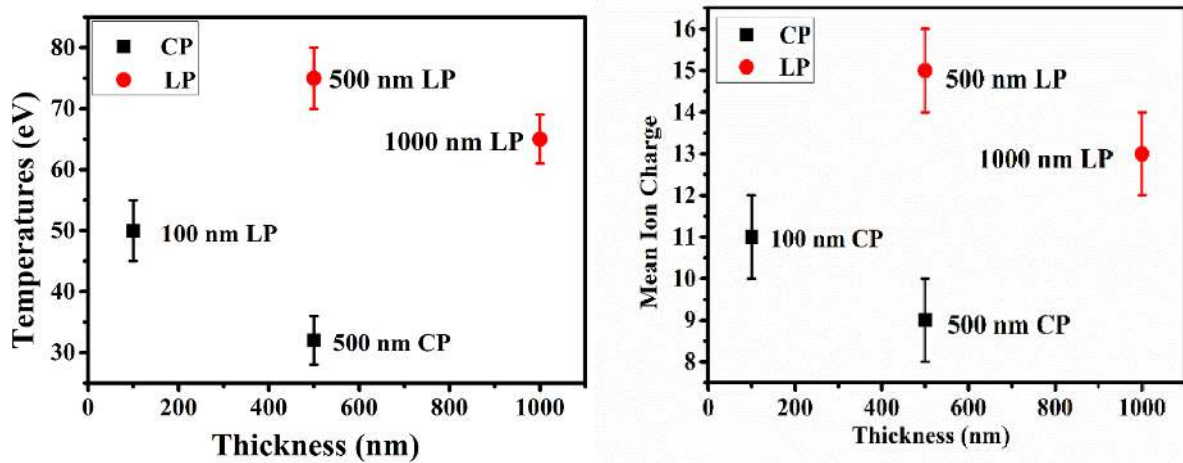


**Figure 6.** Temperature (left) and ionization distribution (right) deduced from FLYCHK for targets of different thicknesses for a density of  $10^{21} \text{ cm}^{-3}$ . The error bars are calculated by considering the shot-to-shot fluctuations and also the error governed by the spectrometer resolution.

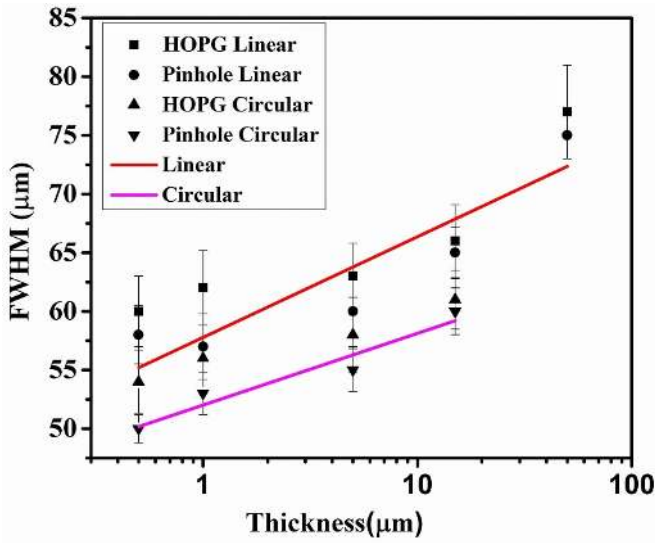
Figures 5(a) and (b) show the experimentally obtained energy spectrum for targets of different thicknesses for different polarizations. Figure 5 (left) compares the  $K\alpha$  energy spectrum emitted from 500 nm and 100 nm Cu targets for a CP laser pulse. It is observed that the energy spectrum is blue-shifted for thinner targets. The thinner dimension of the target allows the target to heat more due to the lesser volume and the resulting higher ionization gives the blue shift. The corresponding photon energies for the 100 nm CP target are 8059.7 eV and 8040.7 eV respectively for  $K\alpha_1$  and  $K\alpha_2$  respectively. When compared to a 500 nm target for CP, a shift of around 7 eV is observed for both  $K\alpha_1$  and  $K\alpha_2$ .

Figure 5 (right) gives a comparison of a 1  $\mu\text{m}$  target with a 500 nm target for LP, which also shows a blueshift for the thinner target. The FLYCHK fitting is also used to observe the temperature and the corresponding ion distribution for different targets having the same laser parameters. Figure 6 shows how the x-ray emission changes with the target thickness. It is observed that the thinner the target, the higher the temperature and consequently the higher the ionization states resulting

in a blue shift in the x-ray emission. Also, the temperature and ionization states are consistently higher for LP laser compared to CP laser.

Although there could be experimental uncertainties due to the shot-to-shot fluctuations and due to the spectrometer resolution, the energy is observed to be always blue-shifted in LP-produced x-rays compared to CP-produced x-rays. In the case of a 500 nm Cu target, the maximum temperature varies between 30 and 80 eV for circular and linear polarization, respectively.

Figure 7 shows the comparison of emission sizes as a function of the polarization of incident light and different thicknesses varying from 500 nm to 50  $\mu\text{m}$ . The measurement of the x-ray source size could be used as a diagnostic tool to infer about the transport of hot electrons within the target. The x-ray source size mainly depends on the divergence of the hot electrons, their propagation, and the stopping distances within the target. It has already been shown that the increase in divergence angle with higher laser intensity is one of the reasons for the increase in source size [40–42]. The motivation for finding



**Figure 7.** FWHM x-ray spot sizes for CP targets and LP targets are shown here from different diagnostics for different polarizations of light. The effect of reduction in source size emission is clearly visible for CP targets. The data points represent an average over the data set for each thickness for clarity over four shots. The uncertainties are calculated based on the measurement error in the x-ray spot size. The solid lines represent a linear fit for both the polarizations for the pinhole data.

the source size for different polarizations with different thicknesses is to perceive the impact of the temperature on the electron's divergence within the target, which in turn dictates the source size.

The FWHM as a function of target thickness is taken as the x-ray source size. The results highlight a dependence of the x-ray source size on the polarization of light. A reduction in source size is clearly visible (figure 7) for CP targets compared to LP targets. The x-ray source size is solely dependent on the global transport of the fast electron beam within the expanded plasma. The fast electron beam propagation and their scattering with cold targets are responsible for generating x-rays. The scattering of the fast electron in a solid is dependent on their temperatures ( $T_h$ ) and their energy ( $E_h$ ) [34, 43, 44]. For targets of the same thicknesses, the obtained source size is higher for LP-produced x-rays in comparison to CP-produced x-rays. The extra thermal agitation makes electron propagation more random and diverged within the plasma for the case of LP-produced x-rays. This extra divergence due to the extra heating is the main reason for the increase in source size in the case of the LP-produced x-rays compared to the CP-produced x-rays. The source sizes are also calculated for different thicknesses of targets for different polarizations of incident light. Hot electrons start with a certain divergence angle and as they penetrate the cold target the spreading of the electrons increases thereby extending the spatial region of interaction with the cold target. As expected, the divergent nature of the electron beam leads to an increase in the size of the emission region with increasing target thickness (increasing from 50  $\mu\text{m}$  diameter for 500 nm thick foils to around 75  $\mu\text{m}$  diameter for the 50  $\mu\text{m}$  thick foils). Overall, the observed source sizes and divergence are within

the variation reported in previously published data where the electron beam divergence has been measured using high Z buried layer targets on targets with 10 s of  $\mu\text{m}$  thickness [45–49].

#### 4. Simulation results

PIC simulations were performed to verify our experimental results for both the polarizations using an open-source code EPOCH [50]. In our 2D simulation, the laser is considered to propagate along the  $+x$ -direction with an intensity similar to that used in the experiment ( $I = 5 \times 10^{19} \text{ W cm}^{-2}$ ). The temporal profile is set to be Gaussian with FWHM 1 ps. The simulation box covers 0  $\mu\text{m}$  to 10  $\mu\text{m}$  along the  $x$ -direction and  $-5 \mu\text{m}$  to  $+5 \mu\text{m}$  along the  $y$ -direction with  $1000 \times 1000$  grid cells. The macro-particles per cell are 32 for both ions and electrons. The electron density for the Cu target was  $n_e = 84.5 \times n_c$ , where  $n_c$  is the critical density of the target corresponding to the wavelength (1.053 nm) of the laser light. Since x-rays are generated within a few time scales of laser pulses, we restricted our simulation time to 5 ps. Bulk electron temperatures are calculated using the electron temperature distribution obtained from the simulation by considering electrons whose energy is below 2.5 KeV [50, 51]. The obtained bulk electron temperature at 2 ps is 39 eV and 80 eV for CP and LP, respectively. Similarly, at 2.5 ps, it is found to be 48 eV and 84 eV for CP and LP, respectively. The simulated results are in good agreement with the experimental results. Figure 8 shows the maximum electron density for both polarizations and electron density is higher in the case of LP

compared to the CP case. The electron density shown in figure 8 is obtained by considering both the hot electrons as well as bulk electrons. Initially, the extra heating in the LP case produces a higher number of hot electrons compared to CP, which is one of the reasons for the observed increase in the electron density. Also, as the hot electrons transfer the energy to the bulk target, the bulk of the target starts to become ionized and the degree of ionization varies with the laser polarization. From the experimental results, it is already observed that higher ionization is the primary reason for the shifting of energy in the case of LP laser. We have already shown that due to the additional component of  $J \times B$  heating in the LP case, the bulk target becomes more ionized compared to the CP case (for LP it is  $15^+$  and for CP it is  $9^+$ ). As the bulk target in the LP case becomes more ionized, it acquires more electron density compared to the CP case. Together, the number of hot electrons as well as the bulk electrons gets increased in the case of LP compared to CP as observed from the electron density plot. The electron density for both cases decreases with time due to multiple reasons, such as, the loss of some of the electrons that escape out of the simulation box from both directions and also due to the onset of hydrodynamic expansion.

Figure 9 shows the electric field and magnetic field variation with time, they are both dominant in nature for the case of LP compared to the CP case. The magnitude of the maximum electric field in the  $x$ - $y$  plane ( $\sqrt{E_x^2 + E_y^2}$ ), and the magnitude of the azimuthal magnetic field ( $B_z$ ) is considered in the above plots. The correspondence between the observed

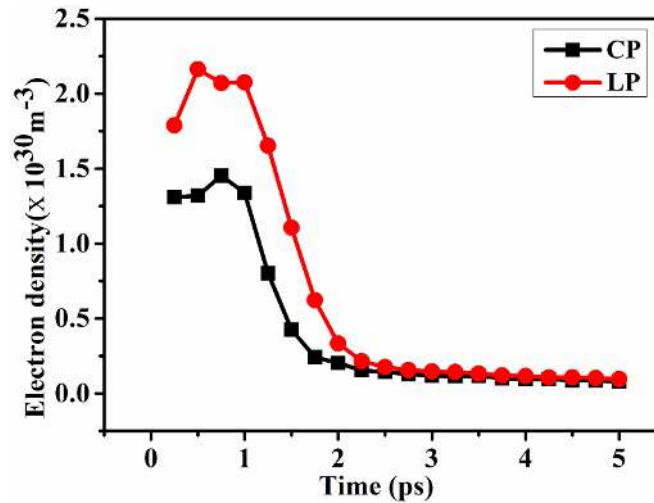


**Figure 8.** Electron density variation with time for a 500 nm Cu foil interacting with laser pulses of different polarization states obtained from 2D PIC simulation EPOCH.

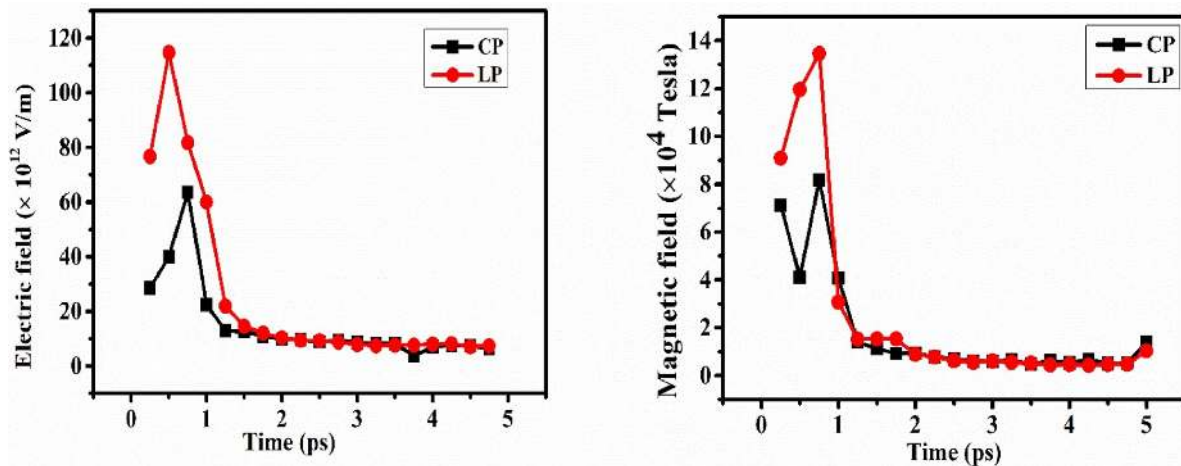


**Figure 9.** The electric field (left) and magnetic field (right) variation with time for a 500 nm Cu foil interacting with laser pulses of different polarizations.

electron density and the electric and magnetic fields could be noticed.

## 5. Conclusion

In conclusion, we have demonstrated an experimental observation for the first time where a variation in the bulk electron temperature of the plasma is dependent on the initial polarization of the laser pulse. These results helped in the understanding of laser coupling mechanisms in different polarization of the laser pulses. This observation is supported by the energy shift in the  $K\alpha$  lines due to the screening effect in higher ionization states. Significant reduction in the source emission size suppressing the global beam spread caused by small-angle scattering for CP is also discussed for various target thicknesses calculated using HOPG and pinhole images. Bulk electron temperature measurements have a direct impact on the neutron yield in ICF experiments. These results are of primary importance for the basic understanding of laser–matter interactions,

especially understanding  $J \times B$  heating in thin targets and for various applications, such as fast ignition fusion, and x-ray backlighters.

## Data availability statement

All data that support the findings of this study are included within the article (and any supplementary files).

## Acknowledgments

We wish to acknowledge: The RAL laser team for providing us the beam time. The usage of EPOCH code which was developed by UK Engineering and Physics Sciences Research Council Grant Nos. EP/G054950/1, EP/G056803/1, EP/G055165/1 and EP/M022463/1. The funding from CRG (CRG/2020/004712) and Imprint Projects (IMP/2019/000275).



## ORCID iDs

B Ramakrishna  <https://orcid.org/0000-0002-2728-6809>  
 K F Kakolee  <https://orcid.org/0000-0001-8180-8113>  
 S Kar  <https://orcid.org/0000-0002-9406-3103>  
 M Cerchez  <https://orcid.org/0000-0002-9294-8397>  
 P McKenna  <https://orcid.org/0000-0001-8061-7091>  
 P A Norreys  <https://orcid.org/0000-0002-5539-9464>

## References

- [1] Strickland D and Mourou G 1985 *Opt. Commun.* **56** 3
- [2] Macchi A, Borghesi M and Passoni M 2013 *Rev. Mod. Phys.* **85** 751
- [3] Arora V, Singhal H, Naik P A and Gupta P D 2011 *J. Appl. Phys.* **110** 083305
- [4] Forslund D W, Kindel J M, Lee K, Lindman E L and Morse R L 1975 *Astrophys. Rev. A* **11** 679
- [5] Brunel F 1987 *Phys. Rev. Lett.* **59** 52
- [6] Denavit J et al 1992 *Phys. Rev. Lett.* **69** 3052–5
- [7] Wilks S C, Kruer W L, Tabak M and Langdon A B 1992 *Phys. Rev. Lett.* **69** 1383
- [8] Brush S, Sahlin H L and Teller E 1966 *J. Chem. Phys.* **45** 2102
- [9] Nantel M, Ma G, Gu S, Côté C Y, Itatani J and Umstadter D 1998 *Phys. Rev. Lett.* **80** 4442
- [10] Lindl J 1995 *Phys. Plasmas* **2** 3933
- [11] Nazir K, Rose S J, Djaoui A, Tallents G J, Holden M G, Norreys P A, Fews P, Zhang J and Failles F 1996 *Appl. Phys. Lett.* **69** 3686
- [12] Park H, Izumi N, Key M H, Koch J A, Landen O L, Patel P K, Phillips T W and Zhang B B 2004 *Rev. Sci. Instrum.* **75** 4048
- [13] Landen O, Glenzer S H, Edwards M J, Lee R W, Collins G W, Cauble R C, Hsing W W and Hammel B A 2001 *J. Quant. Spectrosc. Radiat. Transfer* **71** 465
- [14] Tabak M, Hammer J, Glinsky M E, Kruer W L, Wilks S C, Woodworth J, Campbell E M, Perry M D and Mason R J 1994 *Phys. Plasmas* **1** 1626
- [15] Rathore R, Singhal H and Chakera J A 2019 *J. Appl. Phys.* **126** 105706
- [16] Riley D et al 2005 X-ray scattering from dense plasmas *Plasma Phys. Control. Fusion* **47** B491
- [17] Chen S et al 2007 *Phys. Plasmas* **14** 102701
- [18] Audebert P, Shepherd R, Fournier K B, Peyrusse O, Price D, Lee R, Springer P, Gauthier J-C and Klein L 2002 *Phys. Rev. Lett.* **89** 265001
- [19] Gregori G et al 2005 *Contrib. Plasma Phys.* **45** 284–92
- [20] Neumayer P, Lee H J, Offerman D, Shipton E, Kemp A, Kritcher A L, Döppner T, Back C A and Glenzer S H 2009 *High Energy Density Phys.* **5** 244–8
- [21] Macchi A, Cattani F, Liseykina T V and Cornolti F 2005 *Phys. Rev. Lett.* **94** 165003
- [22] Zhang X, Shen B, Li X, Jin Z and Wang F 2007 *Phys. Plasmas* **14** 073101
- [23] Yan X Q, Lin C, Sheng Z M, Guo Z Y, Liu B C, Lu Y R, Fang J X and Chen J E 2008 *Phys. Rev. Lett.* **100** 135003
- [24] Bi-Cheng L, Xue-Qing Y, Chen L, Yuan-Rong L, Zhi-Yu G, Jia-Xun F, Zheng-Ming S, Yu-Tong L and Jia-Er C 2009 *Chin. Phys. C* **33** 168–70
- [25] Kruer W L and Estabrook K 1985 *Phys. Fluids* **28** 430
- [26] Mulser P and Bauer D 2010 *High Power Laser–Matter Interaction* (Berlin: Springer)
- [27] Macchi A et al 2013 *A Superintense Laser-Plasma Interaction Theory Primer* (Berlin: Springer)
- [28] Gonzalez-Izquierdo B et al 2016 *High Power Laser Sci. Eng.* **4** e33
- [29] Moore A W 1973 *Highly Oriented Pyrolytic Graphite, Chemistry and Physics of Carbon* vol 11 (New York: Marcel Dekker)
- [30] Legall H, Stiel H, Arkadiev V and Bjeoumikhov A A 2006 *Opt. Express* **14** 4570–6
- [31] Yuan X H et al 2011 *Nucl. Instrum. Methods Phys. Res. A* **653** 145–9
- [32] Glenzer S H, Gregori G, Lee R W, Rogers F J, Pollaine S W and Landen O L 2003 *Phys. Rev. Lett.* **90** 175002
- [33] Chung H-K, Chen M H, Morgan W L, Ralchenko Y and Lee R W 2005 *High Energy Density Phys.* **1** 3
- [34] Beg F N, Bell A R, Dangor A E, Danson C N, Fews A P, Glinsky M E, Hammel B A, Lee P, Norreys P A and Tatarakis M 1997 *Phys. Plasmas* **4** 447–57
- [35] Kemp A, Pfund R E W and Meyer-ter-Vehn J 2004 *Phys. Plasmas* **11** 5648
- [36] Salzmann D, Reich C, Uschmann I, Förster E and Gibbon P 2002 *Phys. Rev. E* **65** 36402
- [37] Kemp A, Sentoku Y and Tabak M 2008 *Phys. Rev. Lett.* **101** 075004
- [38] Dromey B et al 2007 *Phys. Rev. Lett.* **99** 085001
- [39] Kluge T, Cowan T, Debus A, Schramm U, Zeil K and Bussmann M 2011 *Phys. Rev. Lett.* **107** 205003
- [40] Zhidkov A G et al 2001 *Phys. Plasmas* **8** 3718–23
- [41] Reich C, Uschmann I, Ewald F, Düsterer S, Lübcke A, Schwoerer H, Sauerbrey R, Förster E and Gibbon P 2003 *Phys. Rev. E* **68** 056408
- [42] Green J S 2008 *Phys. Rev. Lett.* **100** 015003
- [43] Gibbon P and Bell A R 1992 *Phys. Rev. Lett.* **68** 1535
- [44] Kanaya K and Okayama S 1972 *J. Phys. D: Appl. Phys.* **5** 43–58
- [45] Kodama R et al 2004 *Nature* **423** 1005
- [46] Tatarakis M, Davies J R, Lee P, Norreys P A, Kassapakis N G, Beg F N, Bell A R, Haines M G and Dangor A E 1998 *Phys. Rev. Lett.* **81** 999
- [47] Borghesi M, Mackinnon A J, Bell A R, Malka G, Vickers C, Willi O, Davies J R, Pukhov A and Meyer-ter-Vehn J 1999 *Phys. Rev. Lett.* **83** 4309
- [48] Gremillet L et al 1999 *Phys. Rev. Lett.* **83** 5015
- [49] Ramakrishna B et al 2010 *Phys. Rev. Lett.* **105** 135001
- [50] Arber T D et al 2015 *Plasma Phys. Control. Fusion* **57** 113001
- [51] Nishimura H et al 2011 *Phys. Plasmas* **18** 022702